Review Article

Andrés Fabián Lasagni*

Laser interference patterning methods: Possibilities for high-throughput fabrication of periodic surface patterns

DOI 10.1515/aot-2017-0016
Received March 3, 2017; accepted April 3, 2017; previously published online May 10, 2017

Abstract: Fabrication of two- and three-dimensional (2D and 3D) structures in the micro- and nano-range allows a new degree of freedom to the design of materials by tailoring desired material properties and, thus, obtaining a superior functionality. Such complex designs are only possible using novel fabrication techniques with high resolution, even in the nanoscale range. Starting from a simple concept, transferring the shape of an interference pattern directly to the surface of a material, laser interferometric processing methods have been continuously developed. These methods enable the fabrication of repetitive periodic arrays and microstructures by irradiation of the sample surface with coherent beams of light. This article describes the capabilities of laser interference lithographic methods for the treatment of both photoresists and solid materials. Theoretical calculations are used to calculate the intensity distributions of patterns that can be realized by changing the number of interfering laser beams, their polarization, intensity and phase. Finally, different processing systems and configurations are described and, thus, demonstrating the possibility for the fast and precise tailoring of material surface microstructures and topographies on industrial relevant scales as well as several application cases for both methods.

Keywords: direct laser interference patterning; laser interference; laser interference lithography; periodic structures formation; surface functionalization.

***Corresponding author: Andrés Fabián Lasagni,** Institute for Manufacturing Technology, Technische Universität Dresden, George-Baehr-Str.3c, 01069 Dresden, Germany; and Fraunhofer Institute for Werkstoff- und Strahltechnik IWS, Winterbergstrasse 28, 01277 Dresden, Germany,
e-mail: andres_fabian.lasagni@tu-dresden.de

www.degruyter.com/aot

1 Introduction

Surfaces with controlled topographic characteristics can provide enhanced properties in comparison to surfaces with a random roughness [1]. Several examples of ordered topographies can be found on the surfaces of different plants and animals, resulting from several 1000 years of evolution. In this way, nature has shown to be the best technologist to overcome any survival challenge by using bottom-up approaches of patterning.

Laser-based technologies can provide the required technological and economical aspects to reproduce such surfaces using a top-down approach [2]. One technology capable of producing periodic surface structures is laser interference lithography (LIL) [3, 4]. In LIL, the standing wave pattern existing at the intersection of two or more laser beams is used to expose a photosensitive layer such as a resist in a parallel manner. In the case of a negative resist, the positions corresponding to the intensity maxima of the interference pattern are photopolymerized and after development, a periodic variation of the surface topography results. LIL has important advantages compared to other serial lithographic methods such as electron beam lithography (EBL) or ion beam lithography (IBL) including a higher efficiency and a wider workspace. Other advantages include low cost and high throughput, no contamination on the surface as the material is polymerized and not ablated, the capability to fabricate patterns in large areas (up to hundreds of mm in diameter), as well as software-controlled re-configurable patterns (with different periods, feature sizes, and pattern shapes) [4].

If laser systems with sufficient pulse energy are utilized, the irradiated materials can be directly processed. Hence, the method has been called, in this case, direct laser interference patterning (DLIP) [5–10]. Similar to laser-based fabrication methods, the laser radiation can be used to facilitate various metallurgical processes, such as melting, recrystallization or crystallization of amorphous materials. This aspect was

intensively studied in the nineties for silicon [11–13]. Also, the formation of intermetallic phases and grain size architectures has been reported in metals as well as thin films [14, 15].

The most important requirement to produce a periodic structure using DLIP is that the material to be processed must absorb the energy of the laser at the selected wavelength. The laser must provide also sufficient pulse energy (from tens of μJ to some J) to be capable of ablating or modifying the material directly. Depending on the nature of the interaction of the laser light with the used materials, the microstructuring process can be based on mechanisms of photothermal or photochemical nature as well as a combination of both (photophysical ablation) [16, 17].

In this review, the capabilities of LIL and DLIP methods are described. First, calculations of the intensity distribution of interference patterns as a function of the number of beams, polarization, intensity and phase are given. After that, the fabrication of periodic arrays on photopolymerizable materials and solids are described. Also, different processing systems and configurations are described. In all cases, information about the possible resolution is given as well as the areas that can be treated. In particular, for high-throughput/large-volume applications, a new strategy consisting of direct-treating metallic sleeves using DLIP for their use in roll-to-roll embossing methods is introduced. Finally, different applications where LIL and DLIP methods have been used are summarized.

2 Interference principle

Laser interference fabrication methods take advantage of the periodic or quasi-periodic sub-micrometer interference patterns generated by the superposition of two or more coherent light beams, defining one-dimensional (1D), 2D, or even 3D geometries [18].

The electric field resulting from the superimposition of N laser beams can be expressed as:

$$\vec{E} = \sum_{m=1}^{N} \vec{E}_m = \sum_{m=1}^{N} A_m \vec{p}_m \cos(k \vec{n}_m \vec{r} \pm 2\pi\nu t + \phi_m) \quad (1)$$

where A_m is the amplitude, $\vec{p}_m$ is the polarization vector, $k = 2\pi/\lambda$ is the wave number, λ is the wavelength of the laser radiation, $\vec{n}_m$ is the unit vector in the propagation direction, $\vec{r}$ is the position vector, ν is the frequency, and ϕ_m is the phase constant [19].

It can be seen from equation (1), that the electric field is a function of the amplitude, phase, polarization plane, angle of incidence, and wavelength of the N beams (with a minimum of two) and so will be the interference pattern. In a practical LIL configuration, the wavelength of the light source is defined by the laser, and any difference in phase will lead to a spatial translation of the interference pattern. The signal amplitudes of all the beams that are the same as their optical paths are almost the same. In consequence, there are mainly three parameters that will determine the interference pattern [3, 18, 19].

The central parameter determining the geometrical shape of the interference pattern is the number of interfering beams [N in equation (1)]. The angles of incidence of the sub-beams are responsible for the spatial period of the pattern, and the polarization of the beams mainly controls the intensity profile of the interference pattern. In addition, the laser wavelength determines the smallest achievable periodic pattern (i.e. for a two-beam interference pattern $\lambda/2$).

As a result, a huge number of geometries and sizes of the exposed patterns are possible. Some examples of calculated interference patterns with two, three, and four laser beams are shown in Figure 1 [19]. While two laser beams lead to a line-like shape (1D pattern, see Figure 1A and B), three laser beams with different angular positions permit to obtain 2D patterns (Figure 1C–E). For a perfect symmetrical three-beam configuration, a hexagonal arrange can be produced (Figure 1E). Using four laser beams, more complex patterns are possible as shown in Figure 1F–J. The effect of the incident angle on the spatial period is shown in Figure 1A,B,F and G, for a two- and four-beam configuration, respectively (the incident angle is defined as the angle between the laser beam and the line perpendicular to the surface). Although the geometry of the pattern is not affected by the incident angle, larger angles permit to reduce the spatial period (see, for example. Figure 1A,B,F and G) [19].

3 Laser interference lithography

LIL [4, 20] is a maskless fabrication method, which is based on the exposure of a photoresist layer with two or more coherent light beams. Some research groups have referred to this method as interferometric lithography (IL) or holographic lithography [21–24].

LIL has been used to make patterned substrates that are used in a variety of applications including photonic

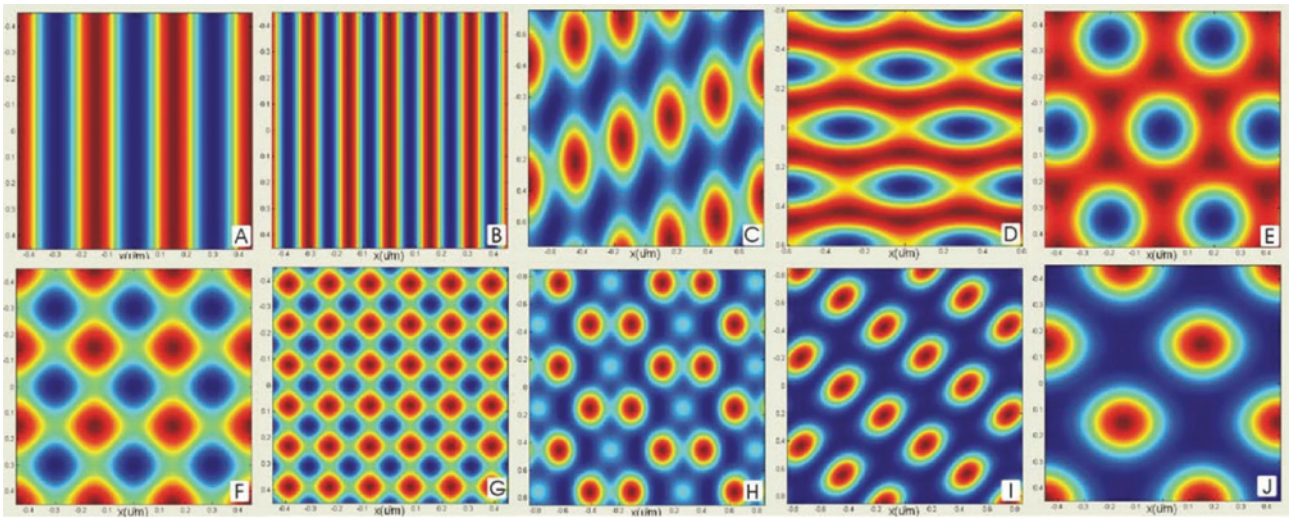

Figure 1: Simulations of interference patterns using: (A and B) two laser beams with different angles of incidence; (C–E) three beams with different angular positions; (F and G) four laser beams with different angles of incidence and (H–J) different angular positions [19]. Red depicts highest dose (intensity maxima positions) and blue the lowest dose.

crystal waveguides, field-emission flat-panel displays, antireflective surfaces, and light-trapping concepts for solar cells [25]. In addition, patterned photoresist structures can be used to form templates for nanoparticle assemblies that can be incorporated into nanophotonic devices [25].

The most important parameters controlling the LIL process include the exposure dosage, the beam power, and the half angle between beams. In addition, optimization of the generated patterns is of great importance, which has been achieved by the application of anti-reflective coating materials, also called bottom anti-reflection coating (BARC) [4, 26]. To simplify the process, a single-beam Lloyd's mirror interferometer is generally used (see Section 5 for additional information) [27]. The wavelength of the laser should match the sensitivity and absorption of the resist. At the same time, the coherence length should be long enough to overcome the optical path length difference. For example, pulsed lasers have coherence lengths in the range of their pulse length, whereas continuous wave (CW) lasers have a very long coherence length (of several meters). CW lasers have the additional advantage that the exposure dose can be easily controlled by varying only the exposure time [26]. The spatial intensity distribution of the pattern is then transferred to a photoresist layer.

An example of a periodic line-like structure produced using two laser beams is shown in Figure 2A [28]. Using this approach, after only a few minutes of UV light exposure, followed by photoresist development and chemical etching, the periodic shape of the pattern could be transferred to the solid Si substrate (spatial period ~500 nm).

To increase the complexity of the periodic structures, two different strategies can be used. For example,

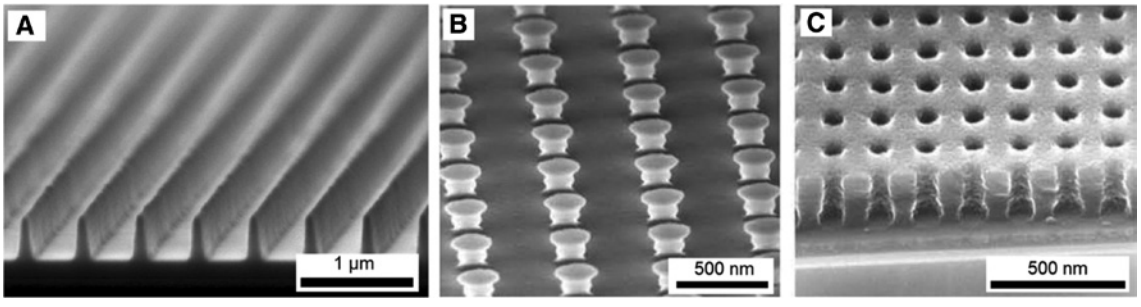

Figure 2: (A) Line-like periodic produced on Si substrate using two-beam LIL after development and chemical etching. The spatial period is approximately 500 nm [28]. Pillar and hole-like patterns produced using double exposure with 90° rotation in (B) positive and (C) negative photoresists [26] (Reprinted with permission from Ref. [26]).

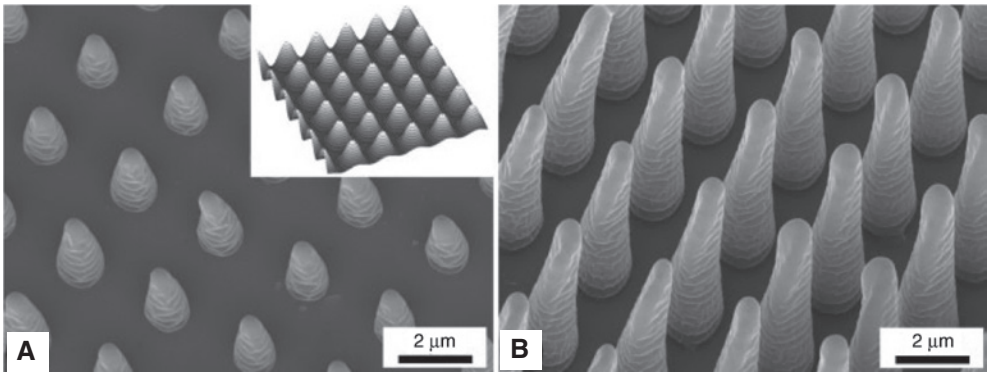

Figure 3: Scanning electron microscope images of PEG-DA pillars fabricated using 95-fs laser pulses and four-beam configuration with exposure dosages of (A) 4.1 and (B) 40.6 J/cm^2. The inset in (A) shows the calculated intensity distribution [29].

rotating the substrate over a certain angle and expose the substrate a second time creates new patterns like isolated lines, cubic and hexagonal structures of pillars and holes. Figure 2B and C shows arrays of pillars and holes, which were produced by rotating the sample 90° degrees between two exposures with the same period. In the example shown in Figure 2B, a positive photoresist was used, which means that the material corresponding to the interference maxima is removed during the development process. On the contrary, if a negative resist is used, such as that shown in Figure 2C, the material is polymerized at the maxima, and thus, the inverse structure is obtained.

The second possibility to increase the complexity of the structures is to use more than two laser beams to produce the interference pattern. As explained in the previous section, this permits to produce a very large amount of geometries, even using only three or four sub-beams.

Figure 3 shows the created periodic structures using a four-beam configuration using two different exposure doses. In this case, a polyethylene glycol diacrylate hydrogel mixed with a photoinitiator (camphorquinone) was irradiated with femtosecond laser pulses with total exposure doses of 4.1 and 40.6 J/cm^2 for Figure 3A and B, respectively [29]. Furthermore, as the utilized material combination is transparent for the used wavelength (800 nm), the photopolymerization process could only be explained by multi-photon absorption, i.e. at a wavelength at which the resist absorbs two or more photons simultaneously (e.g. 400 nm for two-photon absorption).

The experimentally obtained period was 2.85 μm, which is in agreement with the calculated value of 2.96 μm. The calculated intensity distribution of the interference pattern is shown in Figure 3A inset. The height and base width of the fabricated pillars increase with increasing exposure dosage from 1.4 μm and 1.1 μm to 3.0 μm and 1.61 μm, respectively.

Considering the possible resolution of LIL methods, periodic patterns with spatial periods in the sub-micrometer range could be fabricated (i.e. 150–300 nm) using UV laser sources [26]. In addition, areas up to 1.2 m × 1.2 m have been treated with feature sizes between 100 nm and 100 μm [30].

4 Direct laser interference patterning

As mentioned in Section 1, using pulsed laser systems, it is also possible to directly treat solid materials such as metals, ceramics, and polymers. Different from LIL, a binary structuring of the materials (corresponding to periodic patterns with vertical walls) is not possible, as the periodic intensity distribution is generally described by a trigonometric function (i.e. sinus shape for a two-beam setup), which is directly transferred to the material surface. Furthermore, due to the characteristic of the DLIP process, also thermal effects can be locally induced producing thermal gradients and, in some cases, even the flow of material (i.e. when irradiation metals with ns pulses). Therefore, the combination of laser-processing parameters (such laser energy density, pulse duration, laser wavelength) determines the nature of the interaction process with the material obtaining very different structures and geometrical features. In the following, different examples of processed materials with nanosecond, picoseconds, and femtosecond pulses are given.

Nanosecond DLIP: In the case of materials treated with ns pulses (i.e. bulk metals), few laser pulses and large periods produce more homogeneous structures with characteristic sinus-shape topography. For small periods, due to the large thermal conductivity of metals, the heat is easier evacuated from the interference maxima toward the interference minima, and thus, the difference in temperature between this both regions is smaller [31]. This effect makes it difficult to melt the metal only at the interference maxima [6, 15, 32]. Consequently, smaller aspect ratios (quotient between structure height and period) can be achieved.

Examples of typical topographies can be observed in Figure 4. Both line-like and cross-like patterns are produced with a two-beam interference setup (see Figure 4A and C, respectively). For the latter, like in the patterns shown in Figure 2B and D, two irradiations steps are needed, and the substrate was rotated 90°. For the hexagonal arranged patterns of Figure 4B, three laser beams were used. Note that the quality of the structure produced in copper (Figure 4A) is lower than the patterns produced in steel (Figure 4B and C) due to the high thermal conductivity of copper.

Picosecond DLIP: Recently, also ultrashort pulsed laser systems have been used to treat both bulk materials and coatings using DLIP. Compared to ns laser pulses, structures with spatial periods even in the sub-micrometer range can be produced due to the reduced heating of the sample [33].

Examples of treated thin metallic films are depicted in Figure 5. In this case, a four-beam configuration was used. As explained in Section 2, a phase difference between the used beams can lead to changes in the geometry of the interferences pattern [see equation (1)]. If the four laser beams are arranged symmetrically, and the phase difference is set to zero, a quadratic matrix of circular holes is obtained. This case can be observed in Figure 5A and B, where both the Cr and Ag films were totally ablated at the positions corresponding to the interference maxima. If a phase shift of $\pi/2$ occurs between beam pairs, the perfectly ordered hole-like geometry changes to an array of

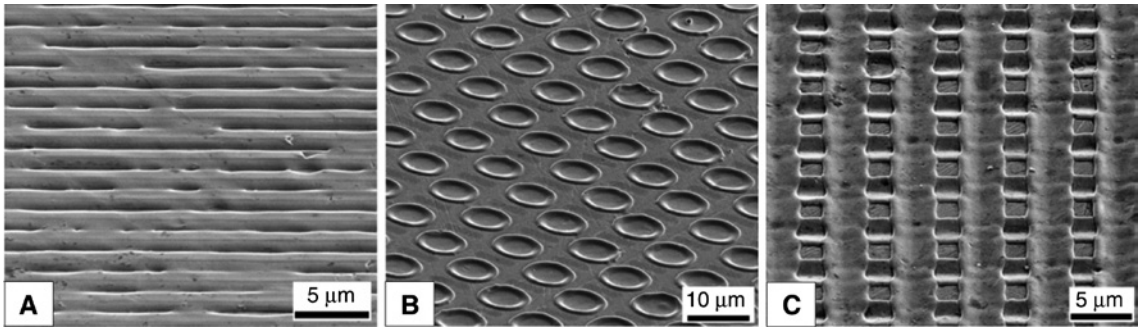

Figure 4: Scanning electron microscope images of treated (A) copper and steel (B and C) using ns-DLIP. In (A), a two-beam configuration was utilized, and the spatial period was 2.0 µm [15]. The hexagonal arrangement in (B) was produced with three laser beams (spatial period: 8.9 µm), while in (C) also two beams were used, but the sample was rotated 90° between the irradiation steps (spatial period: 5.4 µm) [32].

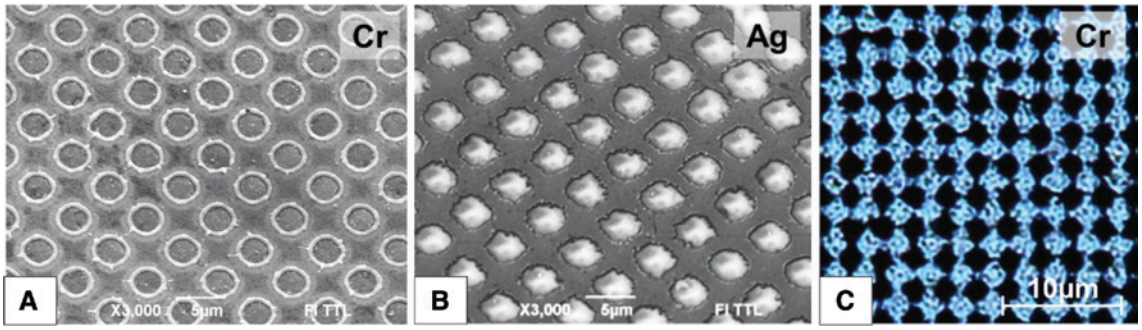

Figure 5: Scanning electron microscope (A, B) and (C) optical microscope images of ps-DLIP-irradiated thin metallic films with four laser beams (100 nm thickness). (A) Cr and (B) Ag films patterned without phase shift between beam pairs. (C) Cr film patterned with a phase shift of $\pi/2$ between beam pairs [33].

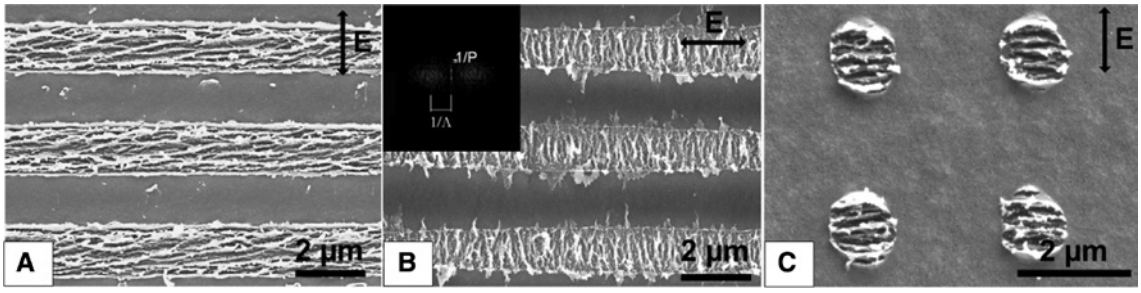

Figure 6: Fabricated (A and B) line-like and (C) crater-like structures on PEDOT:PSS-coated glass substrate using two- and four-beam interference patterns, respectively. The orientation of the electric field *E* is denoted by the black arrow in each figure. Accumulated energy density: (A) 0.21 J/cm^2; (B) 0.35 J/cm^2; (C) 1.56 J/cm^2. The inset in (B) shows the 2D Fourier Transform of the periodic structure with the two periodicities (2.87 μm and 211 nm) [36].

ablated diamond-like shapes (rhombus) as can be seen in Figure 5C.

Femtosecond DLIP: It is common knowledge that the shorter the pulses, the smaller the area over which the pulses overlap. For example, for a 30-fs pulse duration and a moderate angle such as 5°, the beams overlap only within a strip approximately 200 μm wide [34]. However, the overlap can be increased if cross diffraction orders of a grating are crossed using the simple imaging system such as when utilizing a diffractive optical element (DOE) [35].

In this setup, a femtosecond pulse is transmitted through a diffraction grating used as a beam splitter, which is then imaged with two confocal lenses, with the grating being placed in the front focal plane of the first lens. A spatial filter transmits only the desired number of laser beams. Then, the beams are recombined at the image plane.

Using this method, poly(3,4-ethylene dioxythiophene)-poly(styrene sulfonate) (PEDOT–PSS) thin films were treated. A Ti:sapphire fs-laser system with a pulse duration of 95 fs and a center wavelength of 800 nm was utilized. Using two and four beam configurations, different periodic arrays were fabricated (Figure 6). The spatial period in all cases was approximately 2.9 μm [36]. In addition to the periodic structures produced by the interference patterns, also high-frequency arrays, which are orientated perpendicular to the electric field vector, were observed. This sub-wavelength structure was observed for low- and high-energy pulses with a typical size of approximately ~200 nm and could be classified as high spatial frequency laser-induced periodic surface structures (LIPSS). Furthermore, the size of the observed LIPSS does not depend on the period of the produced patterns as its size mainly depends on the nature of the interaction mechanism of the material with the laser light.

A very interesting characteristic of these multi-scale periodic patterns is its similarity with natural examples, such the lotus leaf with super hydrophobic properties. Hence, significantly enhanced surface properties can be obtained by combining a micrometer-scaled structure with nano- or sub-micrometer features [1, 37, 38].

5 Laser interference systems and optical modules

Within the last years, laser interferometric methods have not only shown to be capable of producing functionalized surfaces but also to fulfill an impressive technological development, bringing this technology to real industrial applications. In the following, different processing systems and configurations are described.

Lloyd's mirror interferometer: this equipment is composed of a laser with a long coherent Gaussian beam, lens, pinhole and mirror (Figure 7A). The mirror is placed perpendicular to the exposed substrate to create the second beam [26]. If the substrate and the mirror are placed on a rotating table, the period of the line-like pattern can be easily controlled (the direction of rotation is indicated by the arrow in Figure 7A). The lens and the pinhole are placed into the beam path to create a diverging laser beam. The laser beam should be s-polarized as the reflected and direct beam must have their polarization vectors in the same direction to have optimal interference (high contrast) [26]. This concept is considered to be a one-beam interferometer as the mirror close to the substrate creates the second beam.

Because flat, large-area mirrors are extremely expensive and difficult to handle, the area that is irradiated is typically limited to a few cm^2. Besides, dust particles on the mirror can disturb the interference pattern, thus,

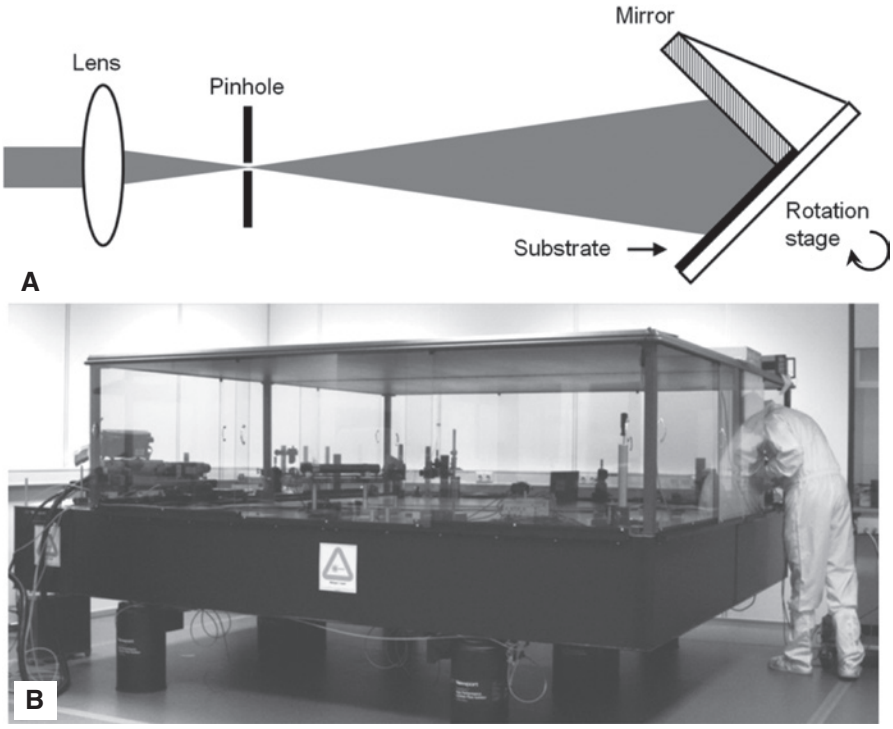

Figure 7: (A) Lloyd's mirror interferometer principle showing the components required to produce the two beam interference pattern for an incident long coherent Gaussian beam (focusing lens, pinhole and mirror) and (B) system on a vibration-controlled table [26].

introducing errors. This setup is not suitable for ultrashort pulse laser systems because the optical delay due to the path beam difference cannot be adjusted [39]. An example of a Lloyd's mirror interferometer system is shown in Figure 7B.

Beam-splitter configuration-based systems: These devices require the use of at least one beam splitter to produce at least two sub-beams, which are later redirected to the surface of the material using mirrors. Here, the longitudinal coherence (narrow spectral width) is important because the distances from the beam splitter to the image plane can vary for the two beams [34, 40]. Phase errors can accumulate when both beams travel long separate paths and encounter different optics, vibrations, mirror imperfections, spurious scattering, and a variety of other deleterious effects [41]. Especially when using CW laser, the effects of both vibration and air turbulences can easily disturb the beams (e.g. for ion-argon lasers). In the last case, the exposure time ranges from some seconds up to several minutes. Thus, a fringe-locking system is generally used to correct fringe movements, which are detected by a photodiode, which actuates a piezoelectrically driven optical element for stabilizing the phase of one of the beams (Figure 8A) [25].

If pulsed laser systems are used, this construction can be done avoiding the fringe-locking system. An example is depicted in Figure 8B [19]. This system can place the last four mirrors before interfering on a virtual circumference. The sample to be treated is placed perpendicular to this circumference. This configuration allows that a longitudinal displacement of the sample and a rotation movement of each mirror will result in a variation of the angle of incidence of the beams. However, after selecting a specific distance between the mirrors and the sample (and, thus, an intercepting angle), the beams have to be positioned at the same area manually.

If ultrashort pulsed laser systems are used, optical delay must be adjusted to superimpose the individual laser beams [39]. However, optical delay is automatically adjusted in the case of interference beam configurations that use transmission beam splitters and a demagnification system or Schwarzschild optics with a coaxial alignment (see Femtosecond DLIP section) [39].

Compact DLIP optical heads and systems: Recently, several concepts of optics for DLIP have been developed. The first alternative to the beam-splitter setup was designed for the fabrication of patterns with a fixed geometry and spatial period. The optical modules consist of a combination of prisms to split the main laser beam followed by cylindrical lenses that permit to reshape the area where the individual sub-beams overlap to a very

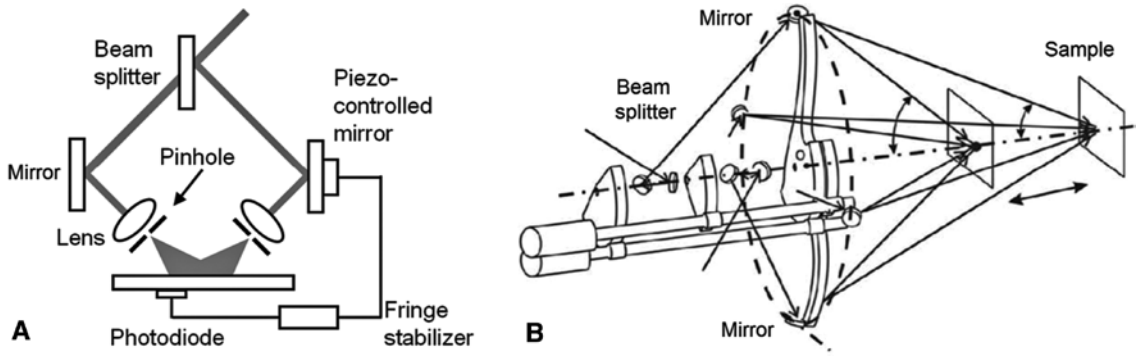

Figure 8: (A) Interference setup with a two-beam configuration with beam splitter using a piezoelectrically controlled mirror for phase stabilization [33] and (B) four-beam direct laser interference system [19].

stretched region (for example, ~15 mm long and 50 µm wide) [42]. This optical module has already achieved impressive fabrication speeds of 0.36 m^2/min on steel and 0.90 m^2/min on polycarbonate (PC) substrates [42].

A second alternative (developed in 2012) is equipped with mobile components to control the intercepting angle between two laser beams automatically. In this case, the incident beam is divided by a diffractive optical element (DOE) into two or four coherent beams of comparable intensities, collimated with a prism or pyramid, and finally recombined using an aspheric lens [43]. Thus, these modules allow to overlap two, three, or four focused laser beams on the substrate where a circular pixel with a diameter varying from 25 µm to 300 µm containing the interference pattern is obtained. Within such a pixel, the interference pattern intensity is transferred into the material surface, and by varying the pattern period, different functionalities can be locally obtained (e.g. different optical colors under a specific observation angle) [2].

Using both above-described modules, compact DLIP systems have been recently developed (see Figure 9). These systems are not only capable of treating planar surfaces (Figure 9A) but also cylinders (or sleeves) up to 600 mm in length and 300 mm in diameter (Figure 9B). The structured sleeves are later used in roll-to-roll embossing systems for high-speed treatment of polymer foils. Up to now, throughputs of 15 m^2/min have been achieved with resolutions up to the submicrometer level, i.e. ~700 nm in Cu, Fe and Ti (the last using 35-ps pulses and a wavelength of 515 nm) [2, 43]. The use of the DLIP method as a tool for the treatment of embossing tools is of important relevance for high-throughput and large-volume applications such as screens or thin film organic solar cells [44].

Up to now, there are efforts underway to pattern large-area metal shims, which can be bent, or direct writing on photosensitive resists on cylinders. However, it is an advantage if direct patterning can be employed without using coating and pattern transfer (etching) processes [45, 46].

A very important issue concerning the large-area DLIP is the lateral uniformity of the produced patterns. Therefore, strategies for positioning of the interference pattern over the surface to be treated during the process must be considered. Figure 10 shows an example of a DLIP-treated

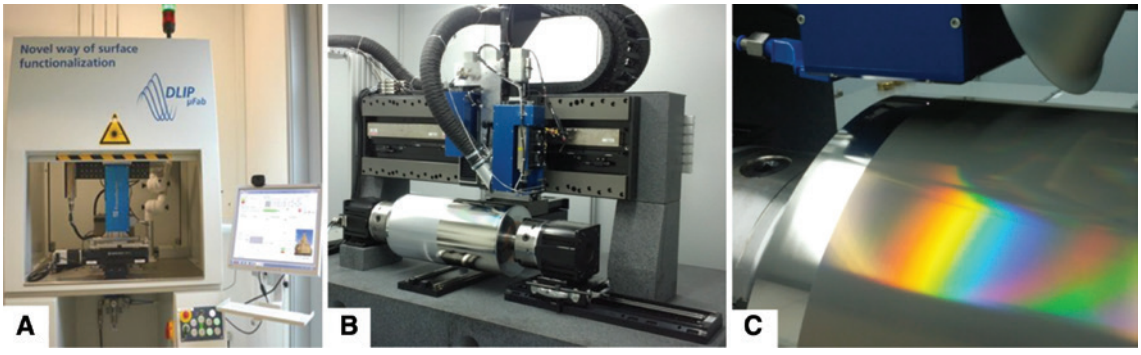

Figure 9: DLIP systems for the treatment of (A) planar surfaces (DLIP-µFAB, Fraunhofer IWS) and (B) large-area sleeves and cylinder for roll-to-roll UV and hot embossing (TU Dresden). (C) Treated Ni sleeve using ps-DLIP.

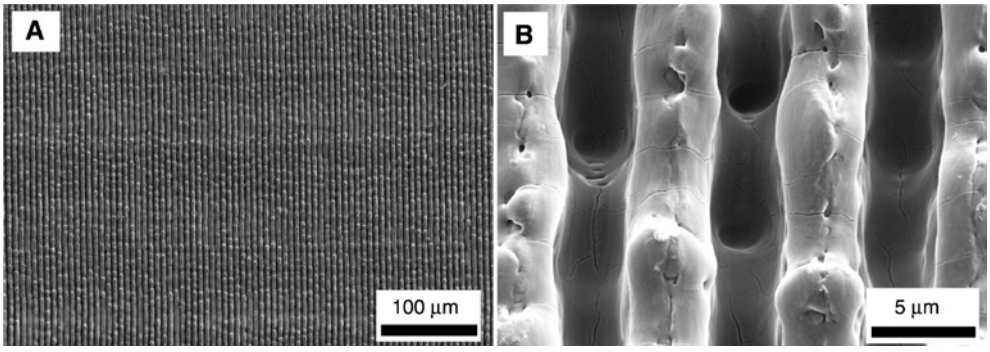

Figure 10: DLIP-treated Ti substrate using pulsed ns-laser systems. The spatial period was 7.1 µm. In (A), a large area is shown, demonstrating a high homogeneity of the pattern over the treated area (note that the DLIP pixel has a diameter of approximately 160 µm). In (B), a detail of the produce surface topography is shown. The observed cracks are typical in Ti when using ns pulses.

Ti substrate with a line-like geometry and a spatial period of 7.1 µm. During the structuring process, the patterns have to be perfectly aligned with the movement direction. Furthermore, in the direction that is perpendicular to the line-like structure, the separation between the laser pulses must be an integer of the spatial period. In the example, the DLIP pixels, with a diameter of approximately 160 µm, were translated 42.6 µm (six times the spatial period) in the mentioned direction. Differently, the pulse-to-pulse distance in the direction parallel to the lines can be freely adjusted (in the example: 8.0 µm). Using this strategy, structures depth of several micrometers can be achieved (i.e. 11.5 µm for 5.2 µm period on stainless steel using 10 ps lasers [47]).

6 Applications of laser interference methods

Both LIL and DLIP methods have been used in the past for a large number of applications.

For example, LIL was used in the fabrication of 2D photonic crystals slabs (PCSs), which are one of the most promising artificial platforms for optical applications such as microcavities, lasers, photodetectors, solar cells, sensors, and reconfigurable photonics [48, 49]. Furthermore, LIL has been also used to produce a large-area anti-reflective coating over Si surfaces for specific ranges of wavelengths [50] as well as an intermediate step to produce plasmonic devices as plasmonic color filters, which are widely used in organic light-emitting diodes (OLEDs), liquid crystal displays (LCDs), and CMOS image sensors [51, 52].

Another interesting application of LIL is for the production of Si nanowires, which have been implemented in field effect transistors, chemical sensors and solar cells [53]. This was possible by combining LIL with metal-assisted etching process.

In the case of DLIP, enhanced tribological performances of surfaces could be proven by producing topographies, which were capable of trapping wear debris and reducing the contact area under dry conditions [54]. Furthermore, DLIP also permitted to prolong the lubrication by a factor of 130 compared with a polished unpatterned steel surface under mixed lubrication [55].

Another application where DLIP has shown high potential is in the functionalization of electrical connectors. By introducing a periodic array in a Sn surface (spatial period ~10 µm), the local contact pressure between the metallic parts could be increased, thus, facilitating the plastic flow of the soft tin layer [56]. As a consequence, the native insulating oxide layer can be removed with a 20% lesser mean surface pressure, leading to a decrease in the electrical contact resistance (ECR) by up to 81% under stationary conditions.

In biology, due to the unique range of micro- and nano-pattern periodicities accessible by DLIP, very specific, on-scale interactions of surface structures and biological cells could be induced. For example, the DLIP technology has demonstrated to be capable of substituting cost-intensive treatment methods (sand blasting, cleaning, and etching) in the preparation of dental implant surfaces [57]. Also, DLIP has been used to produce surfaces showing a significant reduction of bacteria attachment [58].

7 Conclusions

It was shown that laser-based interferometric methods are promising technologies to fabricate defect-free periodic

surface patterns with micrometer and submicrometer resolution on a large variety of materials. The geometry and size of the patterns can be controlled by varying the number of interfering beams and the intensity polarization and phase of each sub-beam. In the case of interference lithography, the versatility of this technique has been demonstrated in both positive and negative photoresists as well as in hydrogel materials. In the case of direct laser interference patterning, direct fabrication of periodic arrays was shown using nanosecond, picosecond, and femtosecond laser pulses.

Also, different processing systems and configurations using the interference principle have been described, demonstrating the possibility for the fast and precise tailoring of material surface microstructures and topographies on industrial relevant scales as well as to produce tools for roll-to-roll imprint processes, which will permit, in the future, a significant reduction of costs of these tools and, thus, of the fabricated products.

Because of the extreme flexibility of interferometric methods in terms of geometries that can be produced, sizes, as well as the large number of materials that can be treated, a large number of applications are possible. These methods have not been only used to improve electronic devices, such as photonic crystals slabs or plasmonic devices, but also on very different application fields such as for the automobile industry by reducing friction or in biology by improving the attachment of cells in implants or reducing the lifetime of bacteria.

Acknowledgments: The work of A.F.L. was supported by the German Research Foundation (DFG), Excellence Initiative by the German federal and state governments to promote top-level research at German universities (Grant no. F-003661-553-41A-1132104). A.F.L. also acknowledges the Bundesministerium für Bildung und Forschung (BMBF) for financial support (Verbundförderprojekt 'Laser Interference High Speed Surface Functionalization', FKZ 13N13113). This work was also partially supported by the Fraunhofer- Gesellschaft under Grant No. Attract 692174.

References

[1] E. Favret and N. Fuentes, in 'Functional Properties of Bio-Inspired Surfaces: Characterization and Technological Applications', (World Scientific Publishing Co. Pte. Ltd., Singapore, 2009).
[2] A. F. Lasagni, T. Kunze, M. Bieda, D. Günther, A. Gärtner, et al., Proc. SPIE 9735, 973515 (2016).
[3] A. F. Lasagni and B. S. Menéndez-Ormaza, Adv. Eng. Mater. 12, 54–60 (2010).
[4] J. H. Seo, J. H. Park, Z. Ma, J. Choi and B.-K. Ju, J. Nanosci. Nanotechnol. 14, 1521–1532 (2014).
[5] A. Lasagni and F. Mücklich, Appl. Surf. Sci. 247, 32–37 (2005).
[6] A. Lasagni and F. Mücklich, Applied Surf. Sci. 240, 214–221 (2005).
[7] F. Yu, F. Muecklich, P. Li, H. Shen, S. Mathur, et al., Biomacromolecules 6, 1160–1167 (2005).
[8] A. Rosenkranz, L. Reinert, C. Gachot and F. Mücklich, Wear 318, 49–61 (2014).
[9] A. Aktag, S. Michalski, L. Yue, R. D. Kirby and S. H. Liou, J. Appl. Phys. 99, 093901 (2006).
[10] L. Guo, H.-B. Jiang, R.-Q. Shao, Y.-L. Zhang, S.-Y. Xie, et al., Carbon 50, 1667–1673 (2012).
[11] C. Nebel, S. Christiansen, H. P. Strunk, B. Dahlheimer, U. Karrer, et al., Phys. Status Solidi (A) 166, 667–674 (1998).
[12] G. Aichmayr, D. Toet, M. Mulato, P. V. Santos, A. Spangenberg, et al., J. Non Cryst. Solids 227, 921–924 (1998).
[13] M. K. Kelly, J. Rogg, C. E. Nebel, M. Stutzmann and S. Kátai, Phys. Status Solidi (A) 166, 651–657 (1998).
[14] F. Muecklich, A. F. Lasagni, C. Daniel, Intermet. 13, 437–442 (2005).
[15] A. F. Lasagni, F. Muecklich, M. R. Nejati and R. Clasen, Adv. Eng. Mater. 8, 580–584 (2006).
[16] M. Bieda, C. Schmädicke, T. Roch and A. F. Lasagni, Adv. Eng. Mater. 17, 102–108 (2015).
[17] A. F. Lasagni, C. Gachot, K. E. Trinh, M. Hans, A. Rosenkranz, et al., Proc. of SPIE 10092, 1009211-1-11 (2017).
[18] M. Ellman, A. Rodríguez, N. Pérez, M. Echeverria, Y. K. Verevkin, et al., Appl. Surf. Sci. 255, 5537–5541 (2009).
[19] A. Rodriguez, M. Echeverría, M. Ellman, N. Perez, Y. K. Verevkin, et al., Microelectron. Eng. 86, 937–940 (2009).
[20] Q. Xie, M. H. Hong, H. L. Tan, G. X. Chen, L. P. Shi, et al., J. Alloys Compd. 449, 261–264 (2008).
[21] M. Campbell, D. N. Sharp, M. T. Harrison, R. G. Denning and A. J. Turberfield, Nature 404, 53 (2000).
[22] A. D. Campo and E. Arzt, Chem. Rev. 108, 911 (2008).
[23] K. Ogai, Y. Kimura, R. Shimizu, J. Fujita and S. Matsui, Appl. Phys. Lett. 66, 1560 (1995).
[24] S. Fujita, S. Maruno, H. Watanabe, Y. Kusumi and M. Ichikawa, Appl. Phys. Lett. 66, 2754 (1995).
[25] L. Cheng, R. Lu and H. Lipson, Laser Photon. Rev. 4, 568–580 (2009).
[26] H. van Wolferen and L. Abelmann, in 'Lithography, Principles, Processes and Materials', (Nova Science Publishers Inc, New York, 2011), ISBN: 978-1-61761-837-6.
[27] J. Choi, M. H. Chung, K. Y. Dong, E. M. Park, D. J. Ham, et al., J. Nanosci. Nanotechnol. 11, 778 (2011).
[28] M. Hong, L. S. Tan, B. Lukyanchuk, L. Shi and T. Chong, in SPIE News room. (2016). doi: 10.1117/2.1200905.1594.
[29] A. F. Lasagni, D. Yuan, P. Shao and S. Das, Adv. Eng. Mater. 11, B20–B24 (2009).
[30] A. Gombert, B. Bläsi, C. Bühler, P. Nitz, J. Mick, et al., Opt. Eng. 43, 2525–2533 (2004).
[31] C. Demuth, M. Bieda, A. Lasagni, A. Mahrle, A. Wetzig, et al., J. Mater. Process. Technol. 212, 689–699 (2012).
[32] M. Duarte, A. Lasagni, R. Giovanelli, J. Narciso, E. Louis, et al., Adv. Eng. Mater. 10, 554–558 (2008).
[33] B. Voisiat, M. Gedvilas, S. Indrišiunas and G. Raciukaitis, Phys. Procedia 12, 116–124 (2011).

[34] A. Lasagni and F. Lasagni, in 'New Trends for Two and Three Dimensional Structures, Advanced Structured Materials Series', (Springer Verlag, Berlin-Heidelberg, 2011).
[35] A. A. Maznev, T. F. Crimmins and K. A. Nelson, Opt. Lett. 23, 1378–1380 (1998).
[36] A. Lasagni, P. Shao, J. L. Hendricks, C. M. Shaw, D. Yuan, et al., Appl. Surf. Sci. 256, 1708–1713 (2010).
[37] W. Barthlott and C. Neinhuis, Planta 202, 1 (1997).
[38] J. Nickerl, M. Tsurkan, R. Hensel, C. Neinhuis and C. Werner, J. R. Soc. Interface 11, 20140619 (2014).
[39] Y. Nakata, Adv. Opt. Technol. 5, 29–38 (2015).
[40] A. F. Lasagni and E. Beyer, in 'Laser Surface Engineering', 1st ed., Ed. By Lawrence and Waugh (Woodhead Publishing, Cambridge), ISBN 978-17824-2074-3.
[41] S. Kuiper, H. van Wolferen, C. van Rijn, W. Nijdam, G. Krijnen, et al., J. Micromech. Microeng. 11, 33–37 (2001).
[42] V. Lang, T. Roch and A. F. Lasagni, Adv. Eng. Mater. 18, 1342–1348 (2016).
[43] M. Bieda, M. Siebold and A. F. Lasagni, Appl. Surf. Sci. 387, 175–182 (2016).
[44] N. Unno and J. Taniguchi, Microelectron. Eng. 88, 2149 (2011).
[45] H. Schift, J. Vac. Sci. Technol. B 26, 458 (2008).
[46] J. Taniguchi and M. Aratani, J. Vac. Sci. Technol. 27, 2841 (2009).
[47] A. F. Lasagni, Proc. of 1. OptecNet Jahrestagung, OpTech-Net e.V., Duisburg (2017).
[48] H. Yang, D. Zhao, S. Chuwongin, J.-H. Seo, W. Yang, et al., Nat. Photonics 6, 617 (2012).
[49] H. Yang, D. Zhao, J.-H. Seo, S. Chuwongin, S. Kim, et al., IEEE Photonics Technol. Lett. 24, 476 (2012).
[50] K. Hadobás, S. Kirsch, A. Carl, M. Acet and E. F. Wassermann, Nanotechnology 11, 161 (2000).
[51] H. S. Lee, Y. T. Yoon, S. S. Lee, S. H. Kim and K. D. Lee, Opt. Express 15, 15457 (2007).
[52] R. W. Sabnis, Displays 20, 119 (1999).
[53] J. de Boor, N. Geyer, J. V. Wittemann, U. Gösele and V. Schmidt, Nanotechnology 21, 095302 (2010).
[54] C. Gachot, A. Rosenkranz, L. Reinert, E. Ramos-Moore, N. Souza, et al., Tribol. Lett. 49, 193–202 (2013).
[55] A. Rosenkranz, T. Heib, C. Gachot and F. Muecklich, Wear 334, 1–12 (2015).
[56] K. E. Trinh, F. Muecklich and E. Ramos-Moore, in 'Proc. 27th Int. Conf. Electr. Contacts', pp. 243–248 (2014).
[57] A. F. Lasagni and D. Guenther, in 'Anwenderforum Funktionale Implantate und Implantatoberflächen', (2015).
[58] A. Rosenkranz, M. Hans, C. Gachot, A. Thome, S. Bonk, et al., Lubricants 4, 2 (2016).